Optimizing Railway Tribology: A Systematic Review and Predictive Modeling of Twin-Disc Testing Parameters

Nicola Zani * , Candida Petrogalli and Davide Battini

Department of Mechanical and Industrial Engineering, University of Brescia, Via Branze, 38, 25123 Brescia, Italy; candida.petrogalli@unibs.it (C.P.); davide.battini@unibs.it (D.B.)
* Correspondence: nicola.zani@unibs.it

Abstract: Twin-disc testing is crucial for understanding wheel–rail interactions in railway systems, but the vast array of testing parameters and conditions makes data interpretation challenging. This review presents a comprehensive analysis of the twin-disc literature experimental data, focusing on how various parameters influence friction and wear characteristics under stationary contaminant conditions. We systematically collected and analyzed data from numerous studies, considering factors such as contact pressure, speed, material hardness, sliding speeds, adhesion, and a range of contaminants. This research showed inconsistent data reporting across different studies and statistical analyses revealed significant correlations between testing parameters and wear rates. For sand-contaminated tests, a correlation between particle size and flow rate was also highlighted. Based on these findings, we developed a simple predictive model for forecasting wear rates under varying conditions. This model achieved an adjusted R^2 of 0.650, demonstrating its potential for optimizing railway component design and maintenance strategies. Our study provides a valuable resource for researchers and practitioners in railway engineering, offering insights into the complex tribological interactions in wheel–rail systems and a tool for predicting wear behavior.

Keywords: twin disc; railway; rail; wheel; wear

1. Introduction

The global transportation sector is undergoing a significant transformation towards greener and more sustainable practices, with public transport systems and particularly railways playing a critical role in this transition. As environmental concerns become increasingly pressing, there is a growing emphasis on reducing the ecological footprint of railway systems [1], including minimizing wear and damage phenomena on critical components such as wheels, rails, and shoe/disc brakes. This reduction in wear not only extends the lifespan of these components but also reduces the need for frequent replacements, thereby conserving resources and lowering emissions associated with manufacturing and maintenance. In this context, understanding and mitigating wear through efficient testing methods becomes vital.

Effectively addressing wear issues in railway systems requires extensive testing to understand the interactions between wheels and rails under various operating conditions. Large-scale testing, while ideal, is often impractical due to high costs and logistical constraints [2–10]. As a result, small-scale testing methodologies such as twin-disc tests and pin-on-disc tests have become invaluable tools in railway research and development [11–16].

Twin-disc tests have gained prominence due to their high proficiency in simulating the contact conditions between wheel and rail surfaces. These tests involve two rotating discs that mimic the wheel–rail interaction, allowing researchers to study wear and friction behaviors with respect to the effects of different materials [17–21], surface treatments [22–27], and lubrication strategies [28–34] on. Twin-disc tests are especially useful for evaluating the impact of various operational parameters, such as load, speed, and environmental conditions,

on wear mechanisms [2,35]. This approach provides critical insights into how different factors contribute to wear and how they can be mitigated through engineering solutions.

The railway industry demands rigorous testing methods to ensure the durability and efficiency of all its components, remarkably when structurally critical. In this regard, twin-disc tests are particularly effective, as they allow for controlled experimentation with various materials and conditions, thus offering a detailed understanding of wear dynamics. These tests play a crucial role in identifying optimal material pairings [19,36,37] and lubrication methods that can significantly reduce wear rates, ultimately contributing to more sustainable railway operations.

The $T\gamma/A$ model, developed by researchers at the University of Sheffield [2,38], has emerged as a widely recognized approach for predicting wear in wheel–rail systems. The model quantifies wear by considering the traction force (T), the slip (γ), and the contact area (A), correlating these parameters with wear rates under various operational conditions. The $T\gamma/A$ index provides a useful framework for understanding the transitions between different wear regimes—mild, severe, and catastrophic—based on the stress and sliding conditions present at the wheel–rail interface. This model has proven effective in mapping wear trends for different material combinations, surface treatments, and environmental conditions, such as contamination by sand or water. It offers a robust method for connecting laboratory-based twin-disc test results to real-world performance, although its application may be limited by the variability in bench configurations and the inherent complexities of full-scale systems. While the $T\gamma/A$ model has provided significant insights into wear prediction, ongoing research continues to refine its applicability and accuracy for more diverse scenarios in railway operations. Rocha et al. [39] reviewed the knowledge and methodologies developed over the past twelve years involving twin disc tribometers. Out of 440 articles from major scientific databases, 133 were selected for analysis using the Bibliometrix tool, identifying key research groups and networks. The study highlighted the twin disc's versatility in simulating railway events like friction management, operational conditions, and evaluating new materials and surface treatments. It also describes the main methodological strategies used in these studies, demonstrating the tool's effectiveness in addressing various railway research themes.

The large number of studies has produced many results, which are difficult to use because they are scattered across various published works. This work systematically collects, catalogs, and organizes data from twin-disc tests conducted over the past decades, creating comprehensive maps that facilitate easy interpretation of test types and their characteristics. The gathered data can be utilized to predict the wear rate based on the assessed conditions. Moreover, it facilitates identifying which test setup parameters seem to significantly affect material performance under operating conditions.

2. Materials and Methods

Literature data from 2008 onwards for twin-disc tests with steady contaminated or uncontaminated conditions (i.e., the same contaminant was used from test start to end or the tests were carried out in dry conditions from the beginning to the end) were collected. The adopted methodology follows the PRISMA checklist; Figure 1 shows the PRISMA flow diagram. When data were in graphic form, the WebPlotDigitizer v.4.6 [40] tool was used for the conversion to numeric data. The following fields were collected when available or calculated when possible: authors, title, journal, nationality, year, type of contaminant used and its characteristics (such as flow rates and size), specimen geometries (radii and thickness), contact characteristics (area, pressure, adhesion coefficient, etc.), linear/rotational and absolute/relative speeds, slip ratio, material names and their microstructure, mechanical properties (initial and final hardnesses, static yield stresses and cyclic yield stresses), various wear metrics, and depths of the layer associated with plastic flow. In order to look for correlations and gather insights on how all the predictors interact with the wear rate, with each other, and how data points are distributed, data will be mostly visualized via scatter plots. Data from all fields were inspected; however, fields that showed no correlation

with wear or damage, and were deemed unlikely to provide useful insights, are omitted to avoid cluttering the paper with irrelevant information.
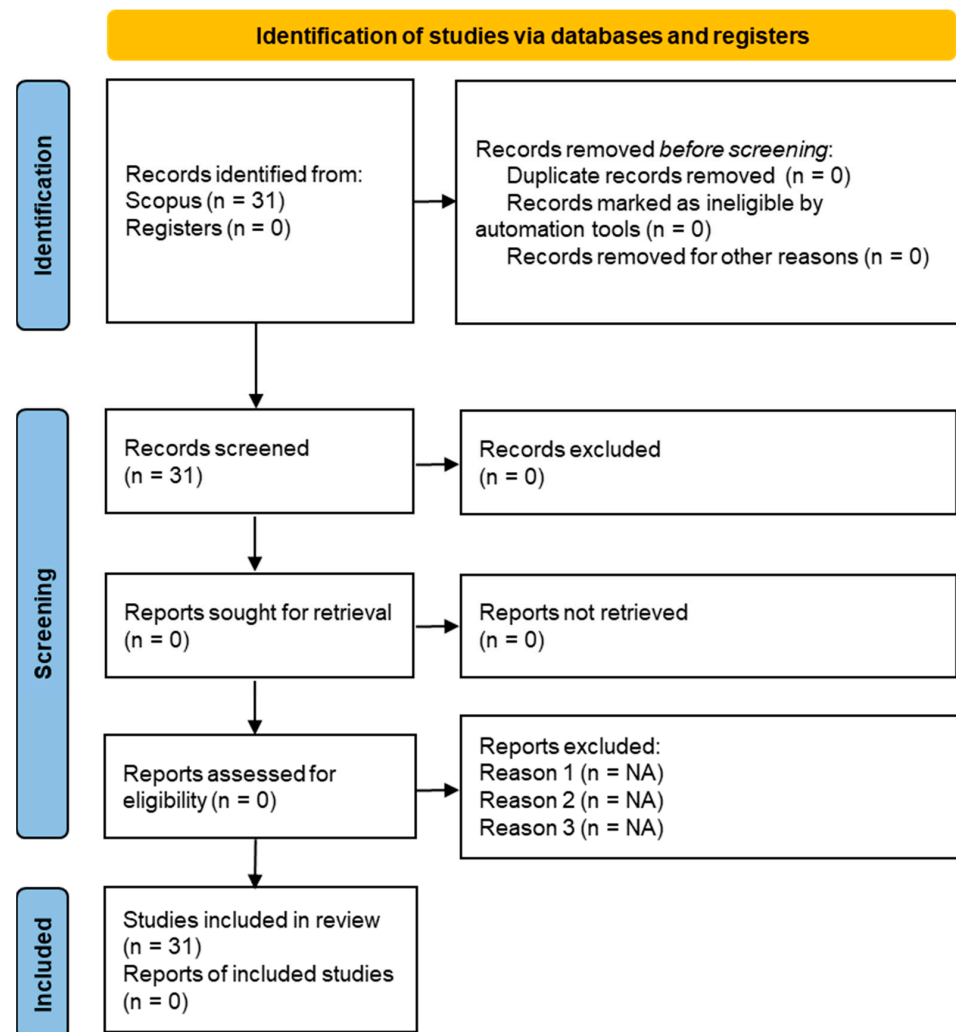

Figure 1. PRISMA flowchart diagram for bibliographic review.

In order to formally express any possible correlation, a stepwise linear model was carried out by setting the p-value thresholds at 0.01 and 0.02 for an F-test of the change in the sum of squared error that results from adding or removing a term respectively. Further model modifications were also checked out manually. The high dimensionality and high cardinality, coupled with the strong sparsity and dispersion of the dataset, suggested not to remove any possible outliers, as their identification would have been trembling. The response variable of the model was defined as the wear rate k, and the predictor variables included were $T\gamma/A$, f (adhesion coefficient), ω (rotating speed of the sample), N_f (number of cycles of the test), contaminant type, and contact type. For each numeric variable, the base-10 logarithm was also considered. Predictors such as static yield, cyclic yield, and others, while being very possibly correlated with the wear rate, were excluded because of their high undefined ratios.

3. Results

Table 1 presents the list of articles analyzed in this paper, along with selected information such as the authors' nationalities, year of publication, and specific test conditions, including contact pressure, sliding speed, and contaminants. The focus is on twin-disc experimental tests where the conditions remain constant throughout the duration of the test.

Therefore, tests involving alternating load conditions, such as an initial dry step followed by the introduction of friction modifiers, are excluded from consideration.

Most of the specimens used in these studies are cylindrical, with some tests using at least one crowned specimen [20,28,41–44]. The limited use of crowned specimens can be attributed to their higher production costs. Additionally, during the test, the transverse radius of a crowned specimen can increase, leading to a decrease in contact pressure [45].

The sliding speed γ [%] is defined as follows [46]:

$$\gamma \ [\%] = 200 \left(\frac{R_W \omega_W - R_R \omega_R}{R_W \omega_W + R_R \omega_R} \right) \tag{1}$$

where R_W and R_R are the radius of the wheel and rail samples along the rolling direction, and ω_W and ω_R stand for the rotational speed of the wheel and the rail specimens.

Regarding the contaminants in play, the analyzed tests predominantly occur under dry conditions. Many studies introduce the contaminant (regardless of its nature) only after an initial dry phase once the adhesion coefficient has stabilized. In some instances, specimens tested under dry conditions are cooled using an air jet to prevent overheating. Beyond tests conducted in clean environments (dry, D), the contaminants studied include liquids such as water (W) and oil (O), as well as solids like sand particles (S), alumina (Al), leaves (L), or grease (G). These contaminants have been analyzed both individually and in combination.

The test conditions are defined in terms of specimen dimensions, pressures, and the contaminants used. Concerning velocities, there is variation in reporting: some researchers specify the velocities of the specimens, while others report only the sliding speed and average velocity. Notably, sliding speed is often expressed in terms of percentages, which could be misleading when comparing studies with specimens of different diameters. To address this issue, the relative sliding speeds have also been converted to absolute sliding speeds in mm/s, ensuring a more robust comparison between different studies.

The scatter plot in Figure 2 illustrates the distribution of the experimental tests concerning the nationalities of the authors and the contaminants studied. This visualization offers a comprehensive overview of the geographic focus and the variety of contaminants considered in the research. Numerous articles have been published without using any contaminants, while others focus on specific contaminants. The most studied contaminants across multiple works are sand, primarily in Italy and China, and water, which has been investigated in Italy, Japan, China, the United Kingdom, and Canada. Other contaminants, whether used alone or combined, have been explored in only a single article or are even limited to a solitary experiment.
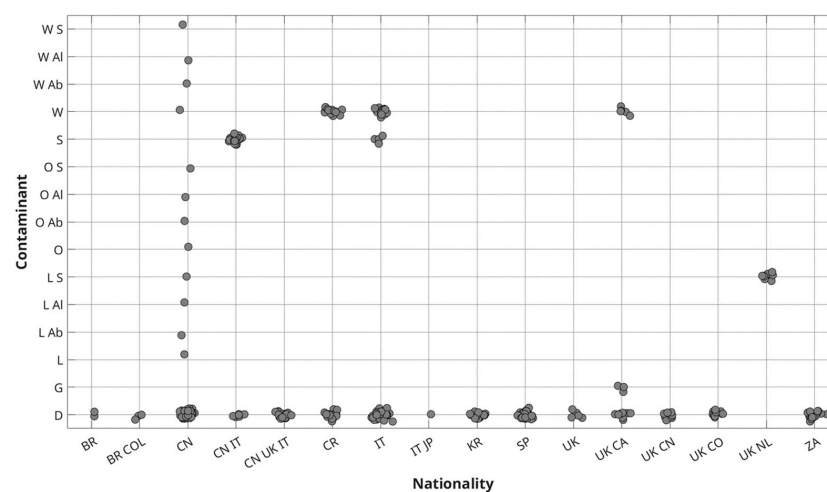

Figure 2. Distribution of article publications by authors' nationality and contaminants. Points are jittered across both axes to facilitate the identification of dense/sparse combinations.

Table 1. List of the collected papers with author's nationalities, applied contact pressures, slip ratio, and contact conditions (D: dry; W: water; S: sand; O: oil; G: grease; L: leaves; Al: alumina; Ab: abrasive).

Paper	Nationality	Year	Contact Pressure [MPa]	γ [%]	Contact Condition
[47]	IT	2008	700, 900, 1100, 1300	0, 0.03, 0.06	D, W
[41]	IT	2015	1100, 1300, 1500	0.24, 1	D
[48]	IT	2017	1100	1	D, W
[49]	IT	2017	1100	0.24, 1	W
[36]	IT	2018	1100	1	D, S
[45]	IT JP	2023	1100	0.05	D
[37]	IT	2024	900, 1100, 1300	0, 1, 3	D
[42]	CN	2016	800, 950, 1000, 1070	2.38	D
[50]	BR COL	2017	1100	5	D
[51]	CN	2016	567	0.17, 0.91, 2.38, 3.83, 9.43	D
[33]	CN	2019	1430	2	D
[20]	BR	2022	3000	0.75	D
[52]	UK CN	2023	1160	0.5, 1, 2, 5	D
[53]	CN	2018	570	0	D
[54]	ZA	2022	552, 740	2, 5, 10, 20, 27	D
[55]	CN IT	2021	1100	1	D, S
[56]	CN UK IT	2021	1500	1	D
[17]	CN UK IT	2020	1500	0.2, 1, 5	D
[57]	CN IT	2022	1100	0.4, 1, 3, 5 , 9	D, S
[58]	KR	2016	1100	0, 0.1, 0.3, 0.5, 1, 1.5	D
[59]	CN	2018	1500	0.5, 1.5, 3, 6, 12, 18, 25	D
[60]	UK	2019	1500	1, 10, 20	D
[29]	UK CA	2014	1500	0, 0.1, 0.3, 0.5, 1, 2, 5, 10, 15, 20	D, W
[61]	KR	2022	1500	1.5	D
[62]	KR	2019	1100	1	D
[63]	SP	2019	690, 920, 1150, 1385	0.1 0.25, 0.5, 0.75, 1, 2, 5	D
[43]	CN	2014	1230	1.95	W, W + S, W + Al, W + Ab O, O + S, O + Al, O + Ab L, L + S, L + Al, L + Ab
[28]	CR	2015	1000	1, 3, 5, 8	D, W
[44]	CN	2016	1274, 1415, 1465	2, 2.38	D
[64]	UK NL	2011	1200	1, 5, 10	L + S
[65]	UK CO	2019	1300	0, 0.5, 1, 1.5, 2, 3, 5, 7, 10, 15, 20	D

Figure 3 depicts the percentage of publications missing reports on specific mechanical properties and results. Notably, properties such as the monotonic and cyclic yield strengths of wheels and rails are frequently omitted, with rail properties being reported less often than those of wheels. Italian researchers are prominent in defining the cyclic properties of wheel steels. This omission may be influenced by collaboration with competitor companies, which can affect the decision to disclose such properties. Moreover, the existing literature lacks

results from twin-disc tests correlated with yield strength. Nevertheless, the (shear) cyclic yield strength is traditionally employed to define the load factor necessary for predicting the cyclic response of the material in shakedown maps [19,37,66–68].
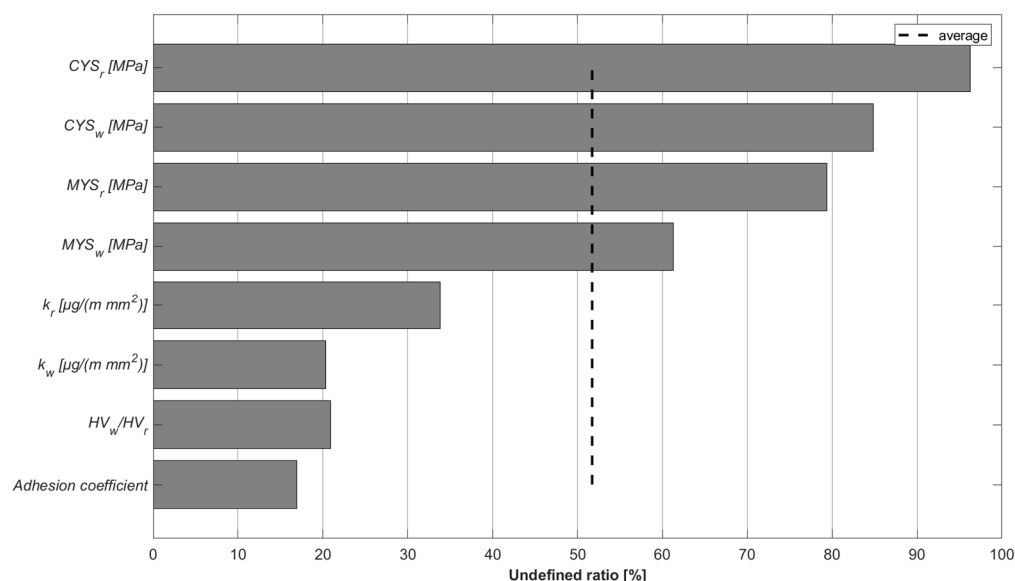

Figure 3. Percentage of missing reports on mechanical properties and results in publications.

In contrast to tensile properties, only about 20% of the studies fail to report the initial hardness of the specimens. However, it is unclear whether these values refer to the average hardness specified by standards for the studied steels or the actual measured values. Regarding the results obtained, wear rates for rails are reported less frequently than those for wheels. Regarding wear rate measurements, some authors reported only the total weight loss at the end of the test, others the weight loss in grams per cycle (g/cycle), and still others in grams per meter per square millimeter (μg/m/mm^2). Where missing and possible, weight loss has been expressed in (μg/m/mm^2) to ensure consistency with the graphs we use. Finally, the adhesion coefficient is usually presented as its stabilized value, or as a variation over the number of cycles. However, it is not always reported, with more than 20% of papers failing to include this.

The histograms in Figure 4 depict the probability distributions of some of the most significant harvested numeric data. The sum of the probabilities (p_i) over all of the (n_B) bins does not lead to one because it relates to the whole population and not to the population subset where each property is defined (i.e. $1 - \sum_i^{n_B} p_i = UR$). As previously mentioned, mechanical properties are often overlooked in these studies.

It is a standard practice to design the wheel–rail system such that the wheel acts as the sacrificial element, resulting in the wheel being softer than the rail. In the tests examined, hardness ratio values (wheel to rail) less than 0.7 and greater than approximately 1.2 are rarely tested, indicating an unevenness in the tribological properties within the wheel–rail system. Most tests are conducted with hardness ratios between 0.8 and 1.2, with a preference for wheels that are softer than the rails. This design choice makes the wheel the sacrificial element in the wheel–rail system, facilitating easier and more cost-effective maintenance [2]. Notably, nearly 90% of the specimens have a diameter between 30 and 60 mm, while approximately 10% of the analyzed tests were conducted with a diameter of 300 mm, which is referenced in a single paper.

Contact pressures vary between 500 MPa and 1500 MPa, with an average value of 1100 MPa and the exception of one study testing a contact pressure of 3000 MPa. As far as the adhesion coefficient is concerned, the histogram shows typical values for the wheel–rail contact interaction, with most of the values being below 0.6. The wear rate values for both wheels and rails have similar distributions even though there are more values reported for

wheels than for rails. The base-10 logarithm was applied to the wear rates because their values are spread across a very wide range, and the choice was corroborated by the look of the resulting distribution.
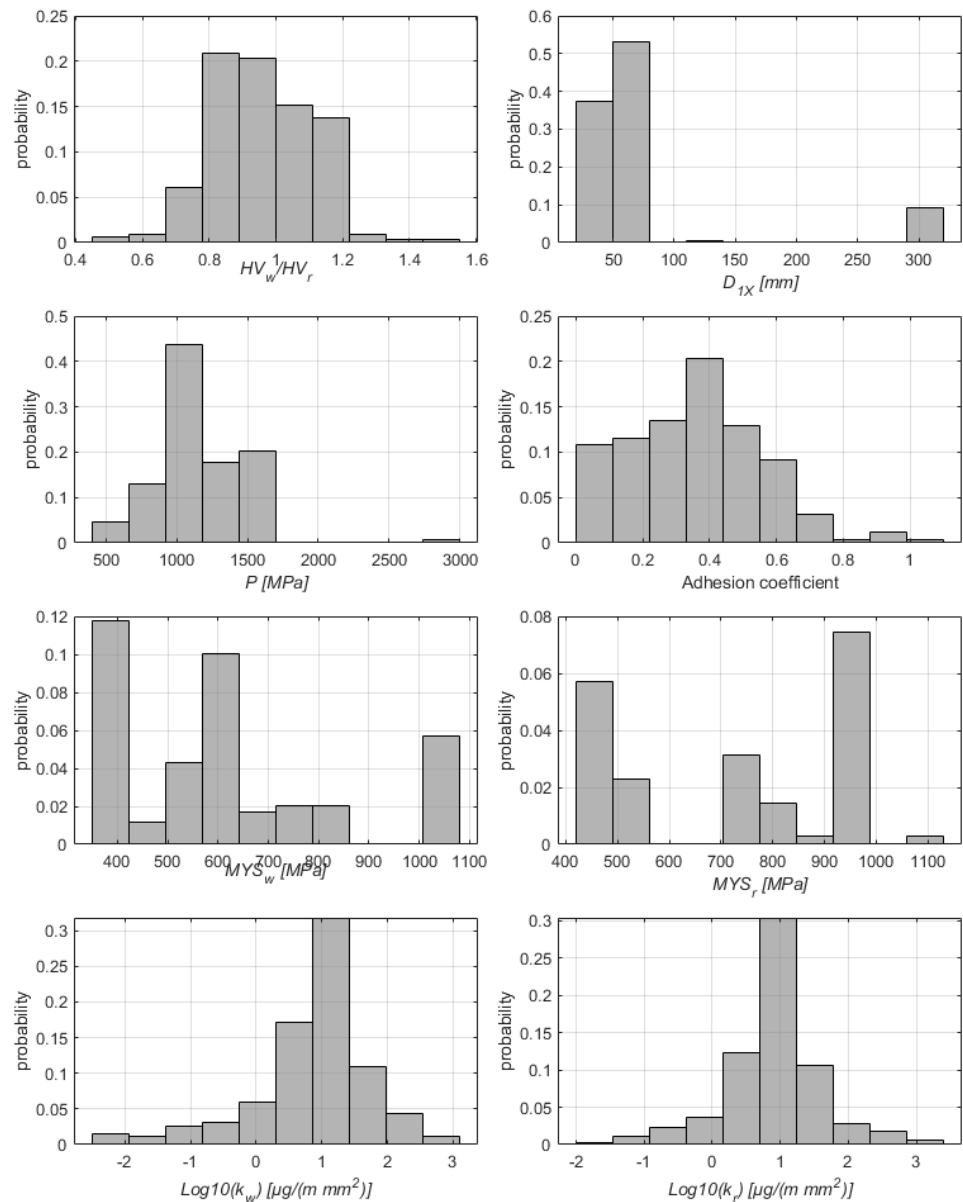

Figure 4. Probability distribution for hardness ratio (HV_w/HV_r), diameter sample along the rolling direction (D_{1X}), contact pressure (P), adhesion coefficient, monotonic yield strength of the wheel and the rail (MYS_w and MYS_r), and logarithmic wheel and rail wear rate ($\log_{10} k_w$ and $\log_{10} k_r$).

The scatter plot in Figure 5 provides a comprehensive analysis of the relationship between $T\gamma/A$ (T is the adhesion force, γ is the slip ratio, and A is the contact area), expressed in N/mm^2, and k, the wear rate measured in µg/m/mm^2. In order to better identify the tests carried out with creepage (γ) approaching the pure rolling, the base-10 logarithmic scale was also adopted for the $T\gamma/A$ parameter. Each data point represents a specific test conducted in various studies, with filled circles representing rail specimens (R) and open triangles representing wheel specimens (W). The data points are color-coded to match different test contaminants. The scatter plot reveals that the wear rate generally rises for both wheel and rail specimens as the average adhesion stress (i.e., T/A) and creepage increase. The majority of tests resulted in a $T\gamma/A$ range of approximately 0.01

to 100 N/mm². Different contaminants exhibit varied effects on wear rate. For instance, tests with the addition of water as a contaminant show lower *k* values, even at higher $T\gamma/A$ values, highlighting water's potential to act as a lubricant and reducing wear rates effectively. In contrast, the application oil combined with alumina (O Al) or other abrasives (O Ab) resulted in a higher wear rate, confirming their foreseeable aggressive material removal capabilities. Oil combined with sand (O S) and pure sand (S) also showed higher wear rates, reinforcing the notion that solid contaminants, whether alone or in conjunction with oil, exacerbate material damage. Finally, the application of sand and leaves together led to the highest wear rate values, with a more detailed discussion of sand-contaminated contact to follow later.
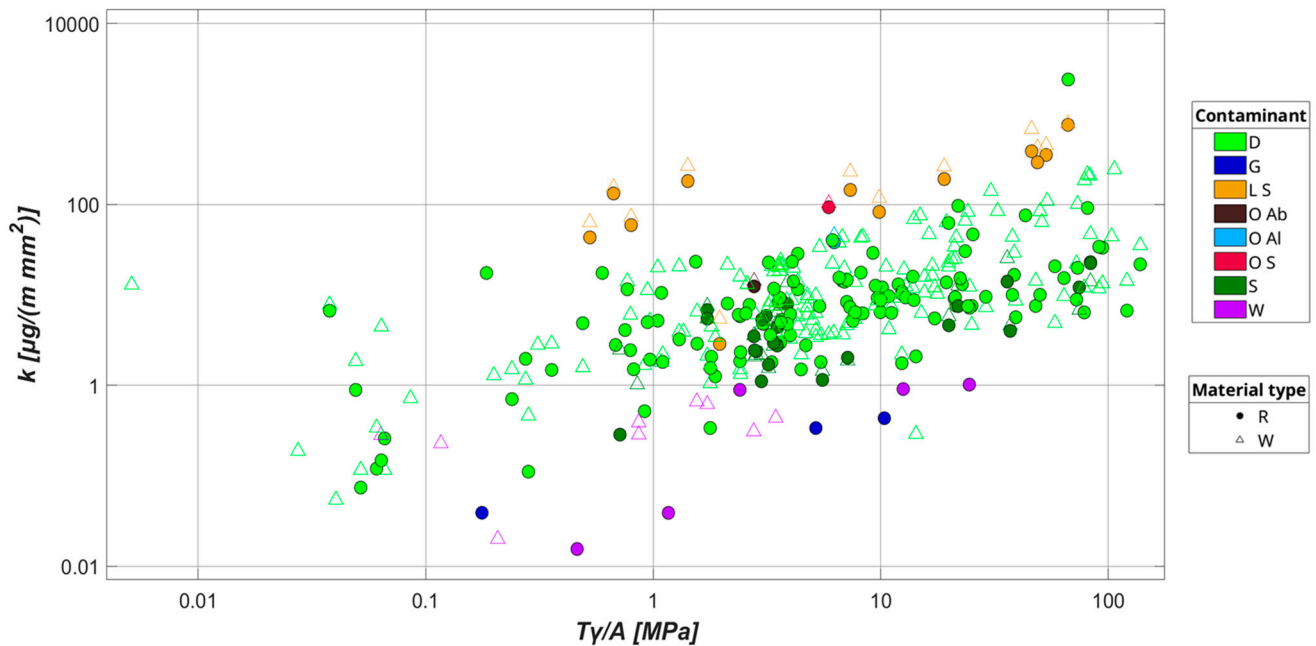

Figure 5. Correlation between the wear rate *k* and $T\gamma/A$ in rail (R) and wheel (W) samples by varying the contaminants (D: dry, G: grease; L S: leaves and sand; O Ab: oil and abrasive; O Al: oil and alumina; O S: oil and sand; S: sand; W: water).

The overlapping distribution of wheel and rail data suggests that similar wear mechanisms might affect both components under certain conditions, underscoring the necessity of optimizing material selection and treatment for both wheels and rails. This observation is crucial for railway engineers looking to design systems that balance wear rates between wheels and rails to maximize longevity and minimize maintenance costs.

Figure 6 shows the dry (D) experiments only while differentiating the cylindrical and crowned specimens. Notably, these results indicate that crowned specimens exhibit wear behavior consistent with that of cylindrical specimens and the color scale highlights that the correlation between *k* and γ is very strong, making the slip ratio the prevailing parameter within the reported $T\gamma/A$ range. As the sliding speed increases, the frictional heating becomes more intense, leading to higher surface temperatures that can soften materials, promote oxidation, and accelerate wear [2,69]. Additionally, faster sliding speeds can induce shifts in wear mechanisms, with adhesive and abrasive wear dominating at low speeds, while oxidative or thermal wear becomes more prevalent at higher speeds [37,38]. Increased sliding velocity also heightens mechanical stresses, contributing to plastic deformation and microfracture formation, further accelerating surface degradation [47].
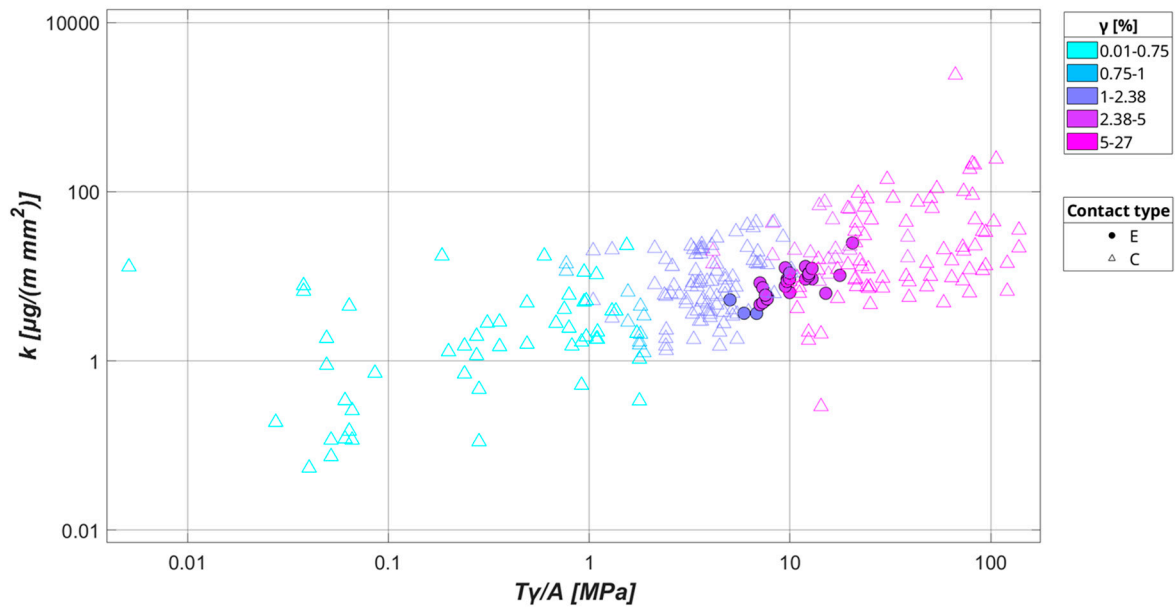
Figure 6. Comparison between cylindrical (C) and elliptical (E) contact. Dry contact conditions only.

Figure 7 illustrates the adhesion coefficient as a function of the type of contaminant and sliding speed. In dry contact tests, those with lower sliding speeds typically exhibit an adhesion coefficient below 0.4, whereas tests conducted at higher sliding speeds generally show values between 0.4 and 0.7. Some experiments with medium sliding speeds report adhesion coefficients greater than 0.8. Remarkably, elliptical contact tests revealed lower adhesion coefficients despite the higher creepage levels used during testing, meaning that higher contact pressure is making up for the low adhesion coefficient to keep $T\gamma/A$ consistent with cylindrical specimens. This effect seems even more prominent when the contact is water-contaminated.
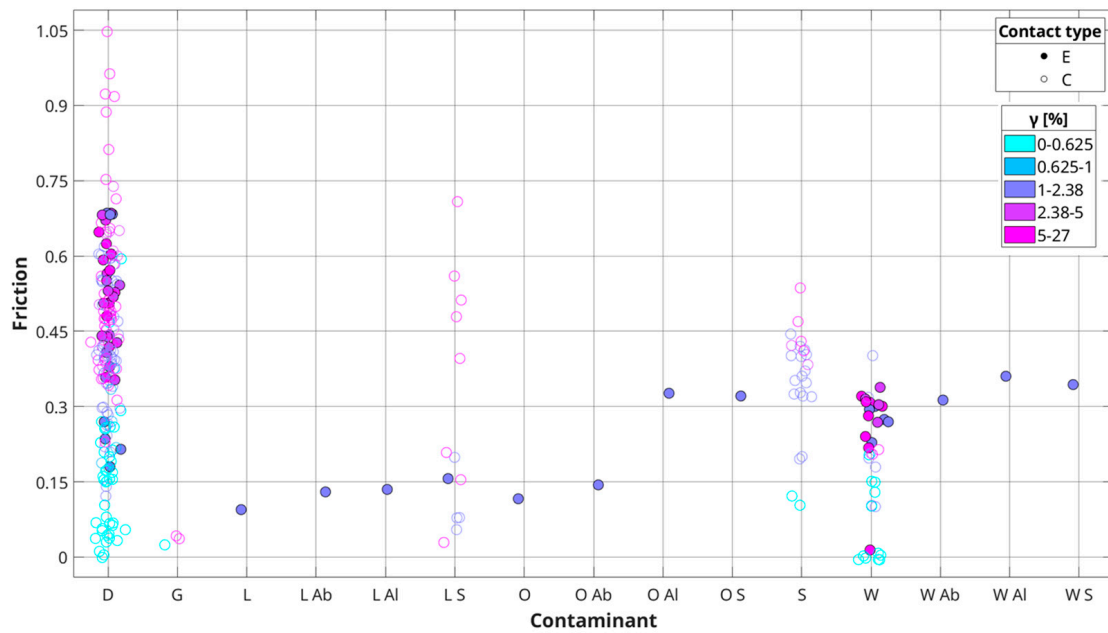

Figure 7. Adhesion coefficient according to the contaminant, the slip ratio, and the contact type.

When examining the tests involving sand and water as individual contaminants, a similar trend is observed: the adhesion tends to increase with higher slip ratios. This behavior can be explained by the role these contaminants play in modifying the contact mechanics.

For sand, its abrasive nature can lead to increased surface roughness and mechanical interlocking, which elevates the adhesion coefficient as sliding speed increases [28,36,70]. When water is involved instead, there is an initial lubrication effect at lower speeds, which is increasingly lacking at higher speeds due to hydrodynamic effects causing the water to not effectively separate the contact surfaces anymore [56]. Analyzing other contaminants proves to be more challenging due to the limited data available, as only a single test is reported for each of the remaining conditions. Nonetheless, the data suggest that the presence of solid contaminants, such as abrasive particles, alumina, or sand, when combined with leaves or liquid contaminants like oil and water, increases the adhesion coefficient. This is likely due to the dual effects of solid particles creating mechanical interlocking and liquids affecting the lubrication regime. The abrasive nature of solids can create micro-scratches on the surfaces, increasing adhesion, while the liquids can vary from acting as a lubricant to facilitating abrasive action, depending on the speed and loading conditions [28,56]. Finally, even if few observations are available, it is particularly noteworthy that grease consistently exhibits the lowest adhesion coefficient of all the contaminants available within the collected data. Grease acts as a highly effective lubricant by forming a thick film that separates the contact surfaces and reduces both the contact adhesion and the surface deformation [28,60].

Figure 8 isolates the water-contaminated tests and shows the relationship between the wear rate and $T\gamma/A$ by highlighting variations in liquid flow rate and slip rate with different markers and colors, respectively. While tests are limited in number, it seems that the wear rate increases, especially for higher slip values of 5% and 10% as the slip rate increases, represented by the shift from blue to pink hues. This suggests a positive correlation between slip rate and wear, confirming that increased slip contributes to higher material wear. On a side note, the three points showing very low wear rates might appear as outliers, but it is not trivial to assess whether this is the case or not when considering data sparsity, numerosity, and dispersion. With all this being considered, there also seem to be limited to no consequences for a significant change in the liquid flow rate. In fact, there is no clear evidence of correlation between the liquid flow rate and the wear rate despite the 2 orders of magnitude difference in flow rate (filled marker for 360 mL/min and hollow ones for 6 ml/min). It is highly likely that the viscosity of water and its ability to form a stable film are related [71,72]. With the flow rates studied, this regime was probably reached. However, proving this conclusively is challenging due to the machine's configuration.
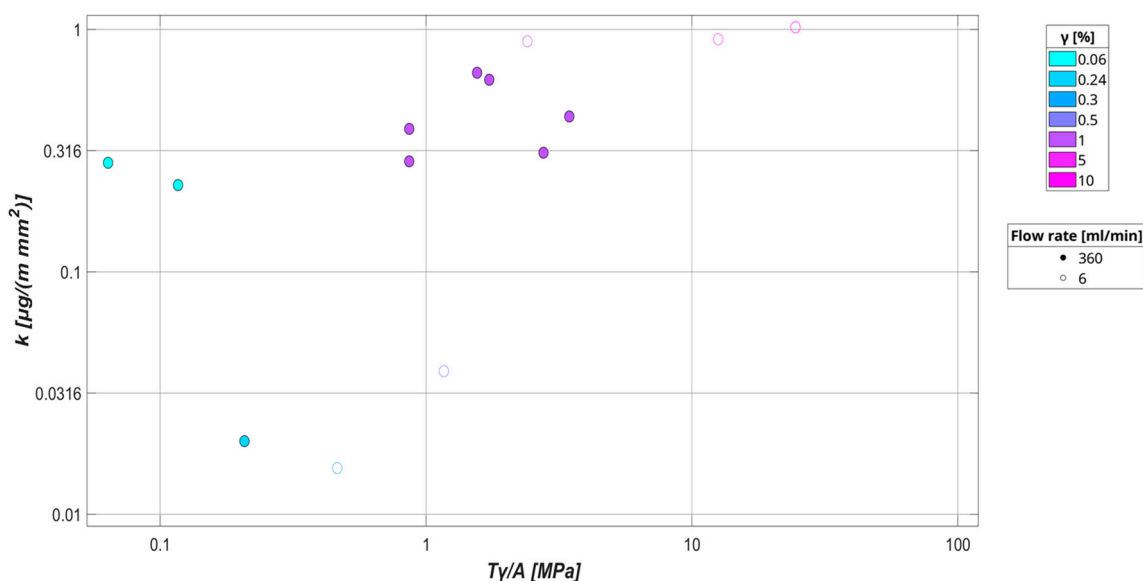

Figure 8. Evolution of wear rate based on $T\gamma/A$ for specimens exposed to water contaminants, considering slip ratio and water flow rate.

Table 2 shows how the various authors applied sand contaminants and which kind of sand they employed. Figure 9a,b illustrate the relationship between $T\gamma/A$ and the wear rate of wheels and rails in tests conducted with sand. These tests analyze the influence of various added contaminants, sand flow, average grain size, and the hardness of the test specimens. While one might expect specimen hardness to be closely related to wear rates, our results show no clear correlation between material hardness and wear rate. Additionally, plotting against the hardness ratio also provided no insights. This is likely due to variations in other experimental conditions across different tests that were not tracked or disclosed. However, tests with leaves and sand (L S) show markedly higher wear rates compared to those with sand (S) alone (Figure 9a). This increase in wear is primarily attributed to two factors: the L S tests involve one of the highest flow rates, and the materials used have among the lowest hardness values. The high flow rate likely intensifies the abrasive action, while the low hardness exacerbates susceptibility to wear [73]. Excluding the sand and leaves tests in Figure 9b, we can state that there are no significant differences in wear between the various contaminants examined. Despite this, we can draw the following conclusions: at equal flow rates, larger grain sizes imply a lower number of particles are being released, and very big grains likely have a higher chance of bouncing away rather than getting crushed and passing through the contact surface. This is consistent with findings from Mazzù et al. [74], who observed that larger particles have a reduced effect on ratcheting and abrasion, as they are less likely to remain in the contact zone and be crushed. On the other hand, smaller grain sizes increase the number of particles that pass through the contact surface, leading to higher abrasion. Moreover, smaller particles have a higher likelihood of becoming embedded in the softer specimen, further contributing to wear by acting as an abrasive agent until they are eventually released. This behavior was highlighted in the computational analysis of solid contaminants, where smaller particles caused deeper surface damage and intensified wear [70,73,74].
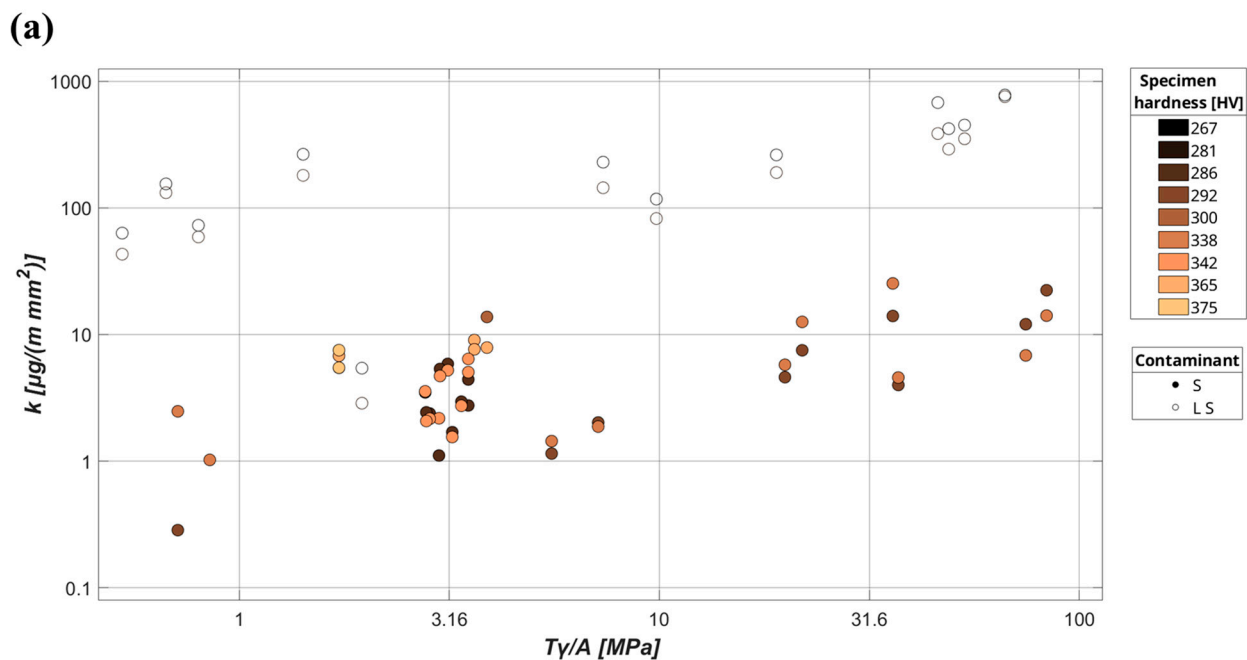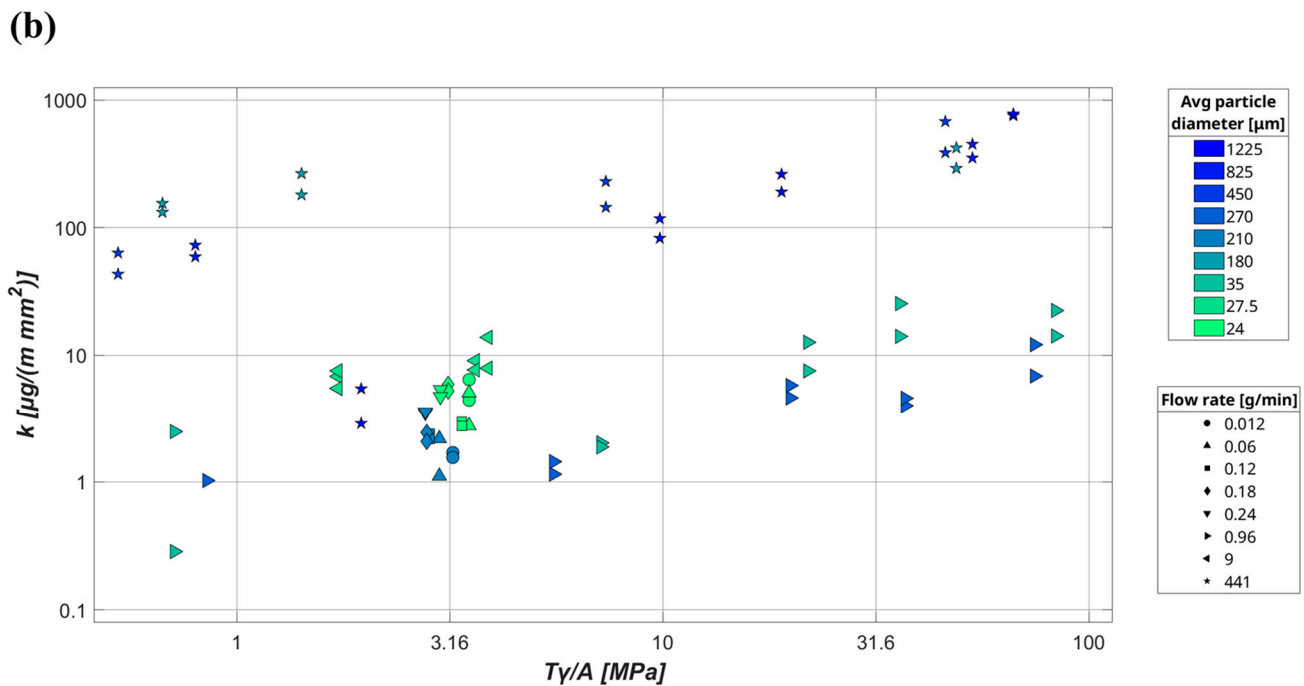
(a)

Figure 9. *Cont.*

(b)

Figure 9. Evolution of wear rate based on $T\gamma/A$ for specimens exposed to sand contaminants, considering (**a**) specimens' hardness and contaminant and (**b**) sand flow rate and average particle dimension.

Table 2. Simulated environmental conditions on the twin disc with sand contaminant.

| Paper	Contaminant	Flow Rate	Average Dimension [μm]	Type of Sand
[64]	L S	441	180, 450, 825, 1225	SiO$_2$ max 96% (pit South Germany, river in the Netherlands)
[36]	S	9	27.5	SiO$_2$ max 86% (commercial sand)
[57]	S	0.96	35, 270	SiO$_2$ Gobi sand, desert sand
[55]	S	0.012, 0.06, 0.12, 0,18, 0.24	24, 210	SiO$_2$ Gobi sand, desert sand
[43]	W S, O S, L S	10	900	Quartz

4. Statistical Investigation

The stepwise linear regression could explain most of the variance with a simple linear model over a log-log scale as per Equation (2):

$$\log_{10} k = a_1 \log_{10} \frac{T\gamma}{A} + a_{2,\,C} \tag{2}$$

where a_1 is fixed and $a_{2,\,C}$ takes on different values depending on the contaminant type (some contaminants were excluded due to their limited number of observations). This model led to an adjusted coefficient of determination R^2_{adj} of 0.650 and a root mean squared error (RMSE) of 0.449 over a total of 365 observations. The estimates and standard deviation of the parameters are reported in Table 3. Figure 10 shows the scatter plots for dry, sand, water, and leaves combined with sand and grease with the regression line(s) and the confidence limits according to Equation (2).

Table 3. Regression parameters for wear rate model (Equation (2)).

Parameter Name	Estimate	Standard Deviation
a_1	0.508	0.030
$a_{2,\,C}\mid_{dry}$	0.531	0.035
$a_{2,\,C}\mid_{grease}$	-0.91	0.26
$a_{2,\,C}\mid_{leaves+sand}$	1.74	0.10
$a_{2,\,C}\mid_{sand}$	0.239	0.079
$a_{2,\,C}\mid_{water}$	-0.64	0.13
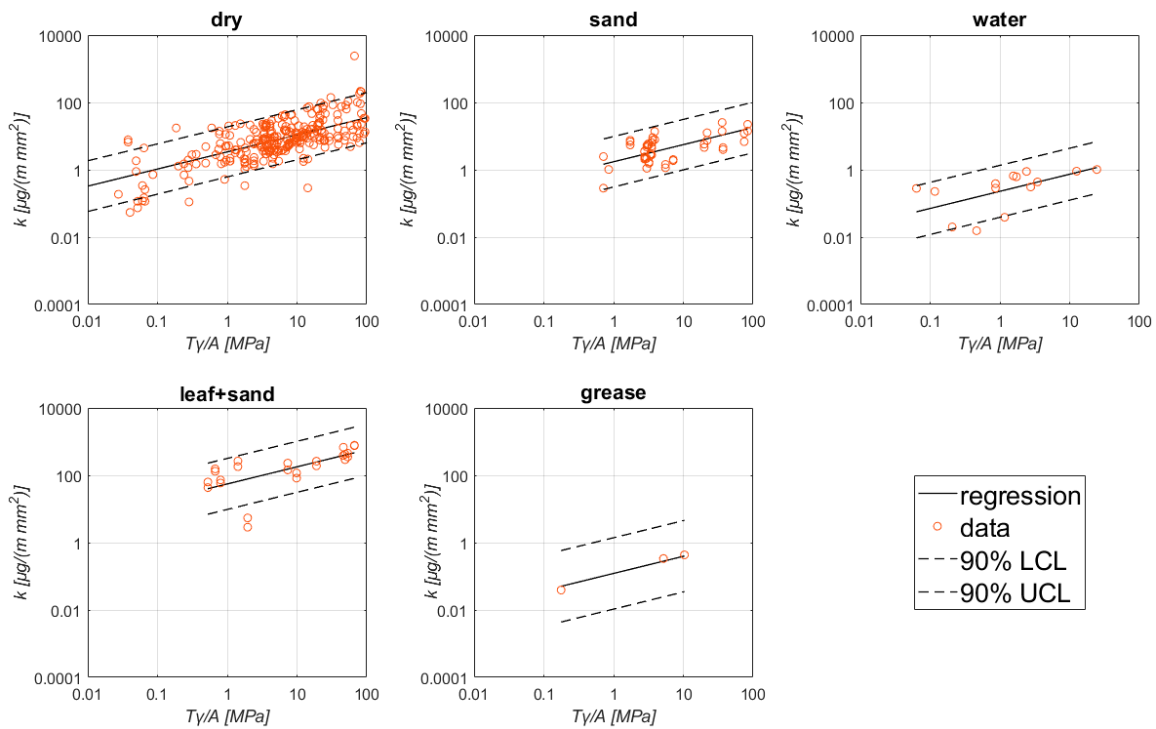
Figure 10. Scatter plots showing the relationship between specific wear rate k and $T\gamma/A$ under different conditions. Each plot includes data points (orange circles), a regression line (solid black), and 90% confidence limits (dashed lines).

While three data points alone are not statistically robust, the inclusion of the grease points highlights a good agreement with the other contaminants, as noticeable in Figure 10, and is also consistent with the selection strategy discussed in Section 2: within a 10-year window and under constant contaminant conditions from test start to end. Although the dry data dominate the regression due to the larger sample size, the overall slope still accommodates all contaminant types, with each contaminant category only leading to significant changes in the intercept. Separate regression trials focused on dry conditions or other specific data subsets, without falling back to datasets comparable to single papers, were also performed but yielded no additional insights.

Adding two more parameters can improve the model accuracy by a limited amount, reaching a coefficient of determination R^2_{adj} of 0.691 and a root mean squared error (RMSE) of 0.422 over the same number of observations. This model includes the linear and quadratic terms for rotational speed, as per Equation (3) and Table 4.

$$\log_{10} k = b_1 \log_{10} \frac{T\gamma}{A} + b_{2,\,C} + b_3\omega + b_4\omega^2 \tag{3}$$

Table 4. Regression parameters for wear rate model (Equation (3)).

Parameter Name	Estimate	Standard Deviation
b_1	0.511	0.029
$b_{2,\,C}|_{dry}$	2.62	0.41
$b_{2,\,C}|_{grease}$	1.31	0.48
$b_{2,\,C}|_{leaves+sand}$	3.97	0.42
$b_{2,\,C}|_{sand}$	2.31	0.41
$b_{2,\,C}|_{water}$	1.43	0.42
b_3	−0.012	0.002
b_4	16.2×10^{-6}	2.5×10^{-6}

As one can imagine, due to data sparsity, dimensionality, and cardinality, the stepwise linear regression can soon lead to overfitting, with this four-parameter model already being harder to interpret and possibly using additional parameters to explain the variance of possible outliers, small clusters of data or simply showing non-causal correlation.

In fact, while still adhering to the p-value thresholds, one could even push the model further and land on seven parameters over five predictors ($\log_{10}(T\gamma/A)$, the rotating speed of the sample ω, the logarithmic number of cycles $\log_{10}\left(N_f\right)$, contaminant type and contact type) as per Equation (4) and Table 5. This approach led to an R^2_{adj} of 0.709 and an RMSE of 0.411 over 345 observations but renders the interpretation even trickier and can most likely be labeled as overfitting, unless proven wrong.

$$\log_{10} k = c_1 \log_{10} \frac{T\gamma}{A} + c_{2,\,C} + c_{3,C} + c_4 + c_5 \log_{10} N_f + c_6\,\omega + c_7\,\omega \log_{10} N_f \qquad (4)$$

Table 5. Regression parameters for wear rate model (Equation (4)).

Parameter Name	Estimate	Standard Deviation
c_1	0.533	0.03
$c_{2,\,C}|_{dry}$	0	0
$c_{2,\,C}|_{grease}$	−1.22	0.24
$c_{2,\,C}|_{leaves+sand}$	2.02	0.15
$c_{2,\,C}|_{sand}$	−0.375	0.069
$c_{2,\,C}|_{water}$	−1.14	0.12
$c_{3,\,C}|_{cylindrical}$	0	0
$c_{3,\,C}|_{elliptical}$	−0.44	0.10
c_4	−10.7	1.5
c_5	2.17	0.31
c_6	0.0233	0.0034
c_7	−0.00440	0.00067

5. Conclusions

This review investigates twin-disc testing parameters for railway applications, focusing on how variables such as test pressure, speed, material hardness, and sliding velocity impact adhesion and wear characteristics under stationary contaminant conditions. By analyzing a vast collection of experimental data, this review elucidates the effects of different contaminants, including oil, grease, sand, and water, on wear mechanisms. The findings highlight the significant influence of contaminant type and flow rate, with certain

contaminants like sand and leaves causing higher wear rates due to their specific properties. Additionally, the study demonstrates that grain sizes and sand flow rates correlate with varying wear behaviors. A predictive model developed from gathered data offers reliable forecasts of wear rates under diverse conditions. This work serves as a valuable resource for understanding the complex interactions in twin-disc systems, ultimately aiding in the optimization and design of railway components to enhance durability and reduce maintenance needs.

This comprehensive analysis of twin-disc testing parameters for railway applications has yielded several important insights:

- The study successfully consolidated and analyzed a vast array of experimental data, providing a unified resource for understanding the complex interactions in wheel–rail tribology.
- Contaminant type and flow rate significantly influence wear mechanisms, with combinations like sand and leaves causing particularly high wear rates.
- For sand contamination, larger grain sizes and higher flow rates were found to correlate with distinct wear behaviors, highlighting the importance of considering particle characteristics in wear predictions.
- A predictive model developed from the collated data demonstrated good accuracy (R^2adj = 0.650) in forecasting wear rates under diverse conditions, offering a valuable tool for railway engineers.
- The study revealed gaps in reporting practices, particularly regarding the mechanical properties of test specimens, highlighting areas for improvement in future research.

These findings have significant implications for the optimization of railway components and maintenance strategies. By providing a deeper understanding of how various parameters influence wear and adhesion, this work enables more informed decision-making in material selection, component design, and maintenance scheduling. The predictive model offers a practical tool for estimating wear rates under specific operating conditions, potentially reducing the need for extensive physical testing.

In conclusion, while the current study has provided valuable insights into the wear behavior of wheel–rail systems using twin-disc testing and the *Tγ/A* model, several limitations remain. One key limitation is that most twin-disc tests are designed to investigate specific conditions, such as a particular load, sliding speed, or contaminant type. As a result, many combinations of parameters—especially those involving varying load ranges, contact pressures, or environmental contaminants—are underrepresented in the available data. This lack of comprehensive testing across a broader spectrum of operating conditions can limit the generalizability of the findings to real-world scenarios, where complex and dynamic interactions occur simultaneously.

Future research should focus on expanding the range of test conditions, particularly by including combinations of loads, speeds, and environmental factors that more accurately represent in-service conditions. Additionally, the development of more advanced wear models that account for microstructural changes, temperature effects, and contact pressure distribution would improve predictive accuracy.

Author Contributions: Conceptualization, N.Z. and C.P.; methodology, N.Z., D.B. and C.P.; data curation, N.Z., D.B. and C.P; writing—original draft preparation, N.Z., D.B. and C.P.; writing—review and editing, N.Z., D.B. and C.P.; visualization, N.Z. and D.B.; supervision, N.Z. All authors have read and agreed to the published version of the manuscript.

Data Availability Statement: Data are available upon request from the authors. The review is registered in the Open Science Framework (https://doi.org/10.17605/OSF.IO/D6KGE, project: Optimizing Railway Tribology: A Systematic Review and Predictive Modeling of Twin-Disc Testing Parameters).

Conflicts of Interest: The authors declare no conflicts of interest.

References

1. European Environment Agency. *Transport and Environment Report 2020: Train or Plane?* Publications Office: Luxembourg, 2021.
2. Lewis, R.; Olofsson, U. *Wheel—Rail Interface Handbook*; Woodhead Publishing Limited: Cambridge, UK, 2009; ISBN 978-1-84569-412-8.
3. Handa, K.; Ikeuchi, K.; Morimoto, F. Temperature-Dependent Wear of Tread-Braked Railway Wheels. *Wear* **2020**, *452–453*, 203265. [CrossRef]
4. Landström, E.V.; Vernersson, T.; Lundén, R. Analysis and Testing of Tread Braked Railway Wheel—Effects of Hot Spots on Wheel Performance. *Int. J. Fatigue* **2024**, *180*, 108116. [CrossRef]
5. Oldknow, K.; Stock, R.; Vollebregt, E. Effects of Rail Hardness on Transverse Profile Evolution and Computed Contact Conditions in a Full-Scale Wheel-Rail Test Rig Evaluation. *Wear* **2024**, *560–561*, 205589. [CrossRef]
6. Zhou, K.; Ding, H.; Wang, W.; Guo, J.; Liu, Q. Surface Integrity during Rail Grinding under Wet Conditions: Full-Scale Experiment and Multi-Grain Grinding Simulation. *Tribol. Int.* **2022**, *165*, 107327. [CrossRef]
7. Wen, J.; Marteau, J.; Bouvier, S.; Risbet, M.; Cristofari, F.; Secordel, P. Comparison of Microstructure Changes Induced in Two Pearlitic Rail Steels Subjected to a Full-Scale Wheel/Rail Contact Rig Test. *Wear* **2020**, *456–457*, 203354. [CrossRef]
8. Buckley-Johnstone, L.E.; Trummer, G.; Voltr, P.; Six, K.; Lewis, R. Full-Scale Testing of Low Adhesion Effects with Small Amounts of Water in the Wheel/Rail Interface. *Tribol. Int.* **2020**, *141*, 105907. [CrossRef]
9. Wu, Y.; Wang, J.; Liu, M.; Jin, X.; Hu, X.; Xiao, X.; Wen, Z. Polygonal Wear Mechanism of High-Speed Wheels Based on Full-Size Wheel-Rail Roller Test Rig. *Wear* **2022**, *494–495*, 204234. [CrossRef]
10. Mädler, K.; Geburtig, T.; Ullrich, D. An Experimental Approach to Determining the Residual Lifetimes of Wheelset Axles on a Full-Scale Wheel-Rail Roller Test Rig. *Int. J. Fatigue* **2016**, *86*, 58–63. [CrossRef]
11. Lyu, Y.; Bergseth, E.; Wahlström, J.; Olofsson, U. A Pin-on-Disc Study on the Tribology of Cast Iron, Sinter and Composite Railway Brake Blocks at Low Temperatures. *Wear* **2019**, *424–425*, 48–52. [CrossRef]
12. Zhu, Y.; Olofsson, U.; Chen, H. Friction Between Wheel and Rail: A Pin-On-Disc Study of Environmental Conditions and Iron Oxides. *Tribol Lett* **2013**, *52*, 327–339. [CrossRef]
13. Ali, N.; Olofsson, U.; Dizdar, S. Friction, Wear, and Airborne Particle Emissions from Rail-Wheel Contact with Laser Cladded Overlays—A Pin-Disc Tribometer Simulation. *Wear* **2023**, *518–519*, 204635. [CrossRef]
14. Mesa, G.D.H.; Vásquez-Chacón, I.A.; Gómez–Guarneros, M.A.; Sanchez-Tizapantzi, P.; Gallardo-Hernández, E.A. A Pin-on-Disk Wear Map of Rail and Wheel Materials from Different Standards. *Mater. Lett.* **2022**, *307*, 131021. [CrossRef]
15. Vásquez-Chacón, I.A.; Sanchez-Tizapantzi, P.; Gómez-Guarneros, M.A.; Enciso-Aguilar, M.A.; Gallardo-Hernández, E.A. Running-in Evaluation after a Rail Grinding Process Using a Pin-on-Disk Tribometer. *Wear* **2023**, *522*, 204686. [CrossRef]
16. Faccoli, M.; Zani, N.; Ghidini, A.; Petrogalli, C. Experimental and Numerical Investigation on the Wear Behavior of High Performance Railway Wheel Steels Paired with Various Brake Block Materials under Dry Sliding Conditions. *Wear* **2022**, *506–507*, 204456. [CrossRef]
17. Hu, Y.; Guo, L.C.; Maiorino, M.; Liu, J.P.; Ding, H.H.; Lewis, R.; Meli, E.; Rindi, A.; Liu, Q.Y.; Wang, W.J. Comparison of Wear and Rolling Contact Fatigue Behaviours of Bainitic and Pearlitic Rails under Various Rolling-Sliding Conditions. *Wear* **2020**, *460–461*, 203455. [CrossRef]
18. Zani, N.; Chaise, T.; Ghidini, A.; Faccoli, M.; Mazzù, A. Numerical study about the effect of bainitic traces on plasticity in ferritic-pearlitic railway wheels. *Proc. Inst. Mech. Eng. Part F J. Rail Rapid Transit* **2020**, *235*, 726–740. [CrossRef]
19. Zani, N.; Petrogalli, C. Predictive Maps for the Rolling Contact Fatigue and Wear Interaction in Railway Wheel Steels. *Wear* **2022**, *510–511*, 204513. [CrossRef]
20. Miranda, R.S.; Rezende, A.B.; Fonseca, S.T.; Fernandes, F.M.; Sinatora, A.; Mei, P.R. Fatigue and Wear Behavior of Pearlitic and Bainitic Microstructures with the Same Chemical Composition and Hardness Using Twin-Disc Tests. *Wear* **2022**, *494–495*, 204253. [CrossRef]
21. Zeng, D.; Qiao, S.; Chen, X.; Gong, Y.; Jiang, B.; Zhao, H.; Zhang, J.; Lu, L. Rolling Contact Fatigue and Wear Behavior of a Vanadium Microalloyed Railway Wheel Steel under Dry Rolling/Sliding Condition. *Int. J. Fatigue* **2024**, *182*, 108207. [CrossRef]
22. Fu, Z.K.; Ding, H.H.; Wang, W.J.; Liu, Q.Y.; Guo, J.; Zhu, M.H. Investigation on Microstructure and Wear Characteristic of Laser Cladding Fe-Based Alloy on Wheel/Rail Materials. *Wear* **2015**, *330–331*, 592–599. [CrossRef]
23. Guo, H.; Wang, Q.; Wang, W.; Guo, J.; Liu, Q.; Zhu, M. Investigation on Wear and Damage Performance of Laser Cladding Co-Based Alloy on Single Wheel or Rail Material. *Wear* **2015**, *328–329*, 329–337. [CrossRef]
24. Wang, C.; Wang, X. Martensite Transformation Characteristics in the Heat Affected Zone of Laser Cladding on Rail. *Mater. Lett.* **2024**, *367*, 136615. [CrossRef]
25. Wang, X.; Zhang, Z.; Zhao, Y.; Hu, Z.; Li, X. Macroscopic Morphology and Properties of Cobalt-Based Laser Cladding Layers on Rail Steel Based on Pulse Shaping. *Opt. Laser Technol.* **2024**, *168*, 109940. [CrossRef]
26. Tomlinson, K.; Fletcher, D.I.; Lewis, R. Evaluation of Laser Cladding as an In-Situ Repair Method on Rail Steel. *Tribol. Int.* **2023**, *180*, 108210. [CrossRef]
27. Meng, L.; Zhu, B.; Xian, C.; Zeng, X.; Hu, Q.; Wang, D. Comparison on the Wear Properties and Rolling Contact Fatigue Damage Behaviors of Rails by Laser Cladding and Laser-Induction Hybrid Cladding. *Wear* **2020**, *458–459*, 203421. [CrossRef]
28. Omasta, M.; Machatka, M.; Smejkal, D.; Hartl, M.; Křupka, I. Influence of Sanding Parameters on Adhesion Recovery in Contaminated Wheel–Rail Contact. *Wear* **2015**, *322–323*, 218–225. [CrossRef]

29. Hardwick, C.; Lewis, R.; Eadie, D.T. Wheel and Rail Wear—Understanding the Effects of Water and Grease. *Wear* **2014**, *314*, 198–204. [CrossRef]

30. Makino, T.; Kato, T.; Hirakawa, K. The Effect of Slip Ratio on the Rolling Contact Fatigue Property of Railway Wheel Steel. *Int. J. Fatigue* **2012**, *36*, 68–79. [CrossRef]

31. Zani, N.; Shu, K.; Ghidini, L.; Petrogalli, C.; Mazzù, A. Impact of Sand Feed Rate on the Damage of Railway Wheel Steels. *IOP Conf. Ser. Mater. Sci. Eng.* **2024**, *1306*, 012036. [CrossRef]

32. Wang, X.; Hua, H.; Peng, K.; Wu, B.; Tang, Z. Study on the Wheel/Rail Adhesion Characteristic under Water and Oil Conditions by Using Mixed Lubrication Model. *Wear* **2024**, *544–545*, 205279. [CrossRef]

33. Liu, J.P.; Li, Y.Q.; Zhou, Q.Y.; Zhang, Y.H.; Hu, Y.; Shi, L.B.; Wang, W.J.; Liu, F.S.; Zhou, S.B.; Tian, C.H. New Insight into the Dry Rolling-Sliding Wear Mechanism of Carbide-Free Bainitic and Pearlitic Steel. *Wear* **2019**, *432–433*, 202943. [CrossRef]

34. Fang, C.; Ding, Y.; Yan, H.; Chen, J.; Zhou, W.; Meng, X. Prediction and Analysis of Wheel Flange Wear on Small Curved Track Considering Wheel-Rail Conformal and Lubricated Contact. *Wear* **2024**, *558–559*, 205569. [CrossRef]

35. Lewis, R.; Olofsson, U. Mapping Rail Wear Regimes and Transitions. *Wear* **2004**, *257*, 721–729. [CrossRef]

36. Faccoli, M.; Petrogalli, C.; Lancini, M.; Ghidini, A.; Mazzù, A. Effect of Desert Sand on Wear and Rolling Contact Fatigue Behaviour of Various Railway Wheel Steels. *Wear* **2018**, *396–397*, 146–161. [CrossRef]

37. Zani, N.; Mazzù, A.; Solazzi, L.; Petrogalli, C. Examining Wear Mechanisms in Railway Wheel Steels: Experimental Insights and Predictive Mapping. *Lubricants* **2024**, *12*, 93. [CrossRef]

38. Bolton, P.J.; Clayton, P. Rolling—Sliding Wear Damage in Rail and Tyre Steels. *Wear* **1984**, *93*, 145–165. [CrossRef]

39. Rocha, R.C.; Ewald, H.; Rezende, A.B.; Fonseca, S.T.; Mei, P.R. Using Twin Disc for Applications in the Railway: A Systematic Review. *J Braz. Soc. Mech. Sci. Eng.* **2023**, *45*, 191. [CrossRef]

40. Rohatgi, A. Webplotdigitizer: Version 4.6 2022. Available online: http://automeris.io/WebPlotDigitizer (accessed on 15 September 2024).

41. Mazzù, A.; Petrogalli, C.; Faccoli, M. An Integrated Model for Competitive Damage Mechanisms Assessment in Railway Wheel Steels. *Wear* **2015**, *322–323*, 181–191. [CrossRef]

42. Ding, H.H.; He, C.G.; Ma, L.; Guo, J.; Liu, Q.Y.; Wang, W.J. Wear Mapping and Transitions in Wheel and Rail Materials under Different Contact Pressure and Sliding Velocity Conditions. *Wear* **2016**, *352–353*, 1–8. [CrossRef]

43. Wang, W.J.; Liu, T.F.; Wang, H.Y.; Liu, Q.Y.; Zhu, M.H.; Jin, X.S. Influence of Friction Modifiers on Improving Adhesion and Surface Damage of Wheel/Rail under Low Adhesion Conditions. *Tribol. Int.* **2014**, *75*, 16–23. [CrossRef]

44. Liu, J.; Jiang, W.; Chen, S.; Liu, Q. Effects of Rail Materials and Axle Loads on the Wear Behavior of Wheel/Rail Steels. *Adv. Mech. Eng.* **2016**, *8*, 168781401665725. [CrossRef]

45. Bodini, I.; Zani, N.; Petrogalli, C.; Mazzù, A.; Kato, T.; Makino, T. Damage Assessment in a Wheel Steel under Alternated Dry-Lubricated Contact by an Innovative Vision System. *Wear* **2023**, *530–531*, 205064. [CrossRef]

46. Fletcher, D.I.; Beynon, J.H. Equilibrium of Crack Growth and Wear Rates during Unlubricated Rolling-Sliding Contact of Pearlitic Rail Steel. *Proc. Inst. Mech. Eng. Part F J. Rail Rapid Transit* **2000**, *214*, 93–105. [CrossRef]

47. Donzella, G.; Faccoli, M.; Ghidini, A.; Mazzù, A.; Roberti, R. The Competitive Role of Wear and RCF in a Rail Steel. *Eng. Fract. Mech.* **2005**, *72*, 287–308. [CrossRef]

48. Faccoli, M.; Petrogalli, C.; Lancini, M.; Ghidini, A.; Mazzù, A. Rolling Contact Fatigue and Wear Behavior of High-Performance Railway Wheel Steels Under Various Rolling-Sliding Contact Conditions. *J. Mater. Eng Perform* **2017**, *26*, 3271–3284. [CrossRef]

49. Mazzù, A.; Petrogalli, C.; Lancini, M.; Ghidini, A.; Faccoli, M. Effect of Wear on Surface Crack Propagation in Rail–Wheel Wet Contact. *J. Mater. Eng Perform* **2018**, *27*, 630–639. [CrossRef]

50. Maya-Johnson, S.; Felipe Santa, J.; Toro, A. Dry and Lubricated Wear of Rail Steel under Rolling Contact Fatigue—Wear Mechanisms and Crack Growth. *Wear* **2017**, *380–381*, 240–250. [CrossRef]

51. Ma, L.; He, C.G.; Zhao, X.J.; Guo, J.; Zhu, Y.; Wang, W.J.; Liu, Q.Y.; Jin, X.S. Study on Wear and Rolling Contact Fatigue Behaviors of Wheel/Rail Materials under Different Slip Ratio Conditions. *Wear* **2016**, *366–367*, 13–26. [CrossRef]

52. Wang, H.H.; Wang, W.J.; Han, Z.Y.; Wang, Y.; Ding, H.H.; Lewis, R.; Lin, Q.; Liu, Q.Y.; Zhou, Z.R. Wear and Rolling Contact Fatigue Competition Mechanism of Different Types of Rail Steels under Various Slip Ratios. *Wear* **2023**, *522*, 204721. [CrossRef]

53. Huang, Y.B.; Shi, L.B.; Zhao, X.J.; Cai, Z.B.; Liu, Q.Y.; Wang, W.J. On the Formation and Damage Mechanism of Rolling Contact Fatigue Surface Cracks of Wheel/Rail under the Dry Condition. *Wear* **2018**, *400–401*, 62–73. [CrossRef]

54. Leso, T.P.; Siyasiya, C.W.; Mostert, R.J.; Moema, J. Study of Rolling Contact Fatigue, Rolling and Sliding Wear of Class B Wheel Steels against R350HT and R260 Rail Steels under Dry Contact Conditions Using the Twin Disc Setup. *Tribol. Int.* **2022**, *174*, 107711. [CrossRef]

55. Shu, K.; Wang, W.; Ding, H.; Lin, Q.; Meli, E.; Guo, J.; Mazzù, A.; Liu, Q. Influence of Sand Transport Rate on Rolling Wear and Damage Behaviors of Wheel/Rail in Gobi and Desert Windblown Sand Environments. *Tribol. Int.* **2022**, *172*, 107584. [CrossRef]

56. Hu, Y.; Watson, M.; Maiorino, M.; Zhou, L.; Wang, W.J.; Ding, H.H.; Lewis, R.; Meli, E.; Rindi, A.; Liu, Q.Y.; et al. Experimental Study on Wear Properties of Wheel and Rail Materials with Different Hardness Values. *Wear* **2021**, *477*, 203831. [CrossRef]

57. Shu, K.; Ding, H.H.; Mazzù, A.; Lin, Q.; Guo, J.; Meli, E.; Liu, Q.Y.; Wang, W.J. Effect of Dynamic Windblown Sand Environments on the Wear and Damage of Wheel-Rail under Different Slip Ratios. *Wear* **2022**, *500–501*, 204349. [CrossRef]

58. Seo, J.-W.; Jun, H.-K.; Kwon, S.-J.; Lee, D.-H. Rolling Contact Fatigue and Wear of Two Different Rail Steels under Rolling–Sliding Contact. *Int. J. Fatigue* **2016**, *83*, 184–194. [CrossRef]

59. Zhu, W.T.; Guo, L.C.; Shi, L.B.; Cai, Z.B.; Li, Q.L.; Liu, Q.Y.; Wang, W.J. Wear and Damage Transitions of Two Kinds of Wheel Materials in the Rolling-Sliding Contact. *Wear* **2018**, *398–399*, 79–89. [CrossRef]

60. Christoforou, P.; Fletcher, D.I.; Lewis, R. Benchmarking of Premium Rail Material Wear. *Wear* **2019**, *436–437*, 202990. [CrossRef]

61. Seo, J.-W.; Hur, H.-M.; Kwon, S.-J. Effect of Mechanical Properties of Rail and Wheel on Wear and Rolling Contact Fatigue. *Metals* **2022**, *12*, 630. [CrossRef]

62. Seo, J.; Kwon, S.; Jun, H.; Lee, C. Effects of Wheel Materials on Wear and Fatigue Damage Behaviors of Wheels/Rails. *Tribol. Trans.* **2019**, *62*, 635–649. [CrossRef]

63. Salas Vicente, F.; Pascual Guillamón, M. Use of the Fatigue Index to Study Rolling Contact Wear. *Wear* **2019**, *436–437*, 203036. [CrossRef]

64. Arias-Cuevas, O.; Li, Z.; Lewis, R. A Laboratory Investigation on the Influence of the Particle Size and Slip during Sanding on the Adhesion and Wear in the Wheel–Rail Contact. *Wear* **2011**, *271*, 14–24. [CrossRef]

65. Santa, J.F.; Cuervo, P.; Christoforou, P.; Harmon, M.; Beagles, A.; Toro, A.; Lewis, R. Twin Disc Assessment of Wear Regime Transitions and Rolling Contact Fatigue in R400HT–E8 Pairs. *Wear* **2019**, *432–433*, 102916. [CrossRef]

66. Xie, Y.; Wang, W.; Guo, J.; An, B.; Chen, R.; Wu, Q.; Bernal, E.; Ding, H.; Spiryagin, M. Rail Rolling Contact Fatigue Response Diagram Construction and Shakedown Map Optimization. *Wear* **2023**, *528–529*, 204964. [CrossRef]

67. Conrado, E.; Foletti, S.; Gorla, C.; Papadopoulos, I.V. Use of Multiaxial Fatigue Criteria and Shakedown Theorems in Thermo-Elastic Rolling–Sliding Contact Problems. *Wear* **2011**, *270*, 344–354. [CrossRef]

68. Johnson, K.L. *Contact Mechanics*; Cambridge University Press: Cambridge, UK, 1985; ISBN 978-1-139-17173-1.

69. Ekberg, A.; Kabo, E. Fatigue of Railway Wheels and Rails under Rolling Contact and Thermal Loading—An Overview. *Wear* **2005**, *258*, 1288–1300. [CrossRef]

70. Grieve, D.G.; Dwyer-Joyce, R.S.; Beynon, J.H. Abrasive Wear of Railway Track by Solid Contaminants. *Proc. Inst. Mech. Eng. Part F J. Rail Rapid Transit* **2001**, *215*, 193–205. [CrossRef]

71. Li, Q.; Wu, B.; Ding, H.; Galas, R.; Kvarda, D.; Liu, Q.; Zhou, Z.; Omasta, M.; Wang, W. Numerical Prediction on the Effect of Friction Modifiers on Adhesion Behaviours in the Wheel-Rail Starved EHL Contact. *Tribol. Int.* **2022**, *170*, 107519. [CrossRef]

72. Skurka, S.; Galas, R.; Omasta, M.; Wu, B.; Ding, H.; Wang, W.-J.; Krupka, I.; Hartl, M. The Performance of Top-of-Rail Products under Water Contamination. *Tribol. Int.* **2023**, *188*, 108872. [CrossRef]

73. Shi, L.B.; Wang, C.; Ding, H.H.; Kvarda, D.; Galas, R.; Omasta, M.; Wang, W.J.; Liu, Q.Y.; Hartl, M. Laboratory Investigation on the Particle-Size Effects in Railway Sanding: Comparisons between Standard Sand and Its Micro Fragments. *Tribol. Int.* **2020**, *146*, 106259. [CrossRef]

74. Mazzù, A.; Battini, D.; Zani, N. Computational Assessment of Ratcheting in Rail-Wheel Contact with Solid Contaminant. *Wear* **2024**, *546–547*, 205346. [CrossRef]